Orbital forcing of the martian polar layered deposits

Jacques Laskar*, Benjamin Levrard* & John F. Mustard†

** Astronomie et Systèmes Dynamiques, IMC-CNRS UMR8028, 77 Av. Denfert-Rochereau, 75014 Paris, France*
† Department of Geological Sciences, Brown University, Providence, Rhode Island 02912, USA

Since the first images of polar regions on Mars revealed alternating bright and dark layers, there has been speculation that their formation might be tied to the planet's orbital climate forcing[1–4]. But uncertainties in the deposition timescale exceed two orders of magnitude: estimates based on assumptions of dust deposition, ice formation and sublimation, and their variations with orbital forcing suggest a deposition rate of 10^{-3} to 10^{-2} cm yr^{-1} (refs 5, 6), whereas estimates based on cratering rate result in values as high as 0.1 to 0.2 cm yr^{-1} (ref. 7). Here we use a combination of high-resolution images of the polar layered terrains[8], high-resolution topography[9] and revised calculations of the orbital and rotational parameters of Mars to show that a correlation exists between ice-layer radiance as a function of depth (obtained from photometric data of the images of the layered terrains) and the insolation variations in summer at the martian north pole, similar to what has been shown for palaeoclimate studies of the Earth[10–12]. For the best fit between the radiance profile and the simulated insolation parameters, we obtain an average deposition rate of 0.05 cm yr^{-1} for the top 250 m of deposits on the ice cap of the north pole of Mars.

Of the Mars Orbiter camera (MOC) images acquired of both the north and south polar regions, only a fraction clearly resolve layering, owing to the limited exposure of layers in troughs, seasonal frosts, image quality or illumination conditions. We focus on one particular image (M00-02100; see Fig. 1) from the north polar cap because of its high quality and the length of section exposed. Although layers are exposed in the southern cap, the length of any section is too short to be useful. The layers evident in image M00-02100 are representative of one long trough in the northern cap located near 279° W 86° N, from which several other MOC images were acquired; these layers show a consistent stratigraphy over a strike of more than 100 km.

The actual composition of the polar layers is poorly known. The residual north polar cap consists largely of water ice, although a 1–2-m-thick layer of CO_2 ice is formed and removed annually[13]. The darkening agent is thought to be dust or low-albedo sands and the general interpretation is that the layers are formed of frozen volatiles (mainly water) and dust deposited by atmospheric suspension (for example, see ref. 3).

The reflected intensity varies with local slope, dust and water/ice proportions, and season (owing to CO_2 frost deposition in winter, and differential retention of CO_2 and H_2O ice in summer). Images M00-02100 and E03-02206 (one martian year later), both acquired in midsummer from the same trough, show an identical pattern of light and dark bands. The early springtime image M18-00804 does not show intensity reversals relative to the summer images, which suggests the absence of stair steps and of significant short-scale slope effects on the summer albedo profile[14]. Regardless of the actual origin of the intensity contrasts that define the layers in the images (textural, composition, illumination), they display regular patterns of reflectance with depth that can be used to test the orbital forcing theory.

Profiles of radiance were extracted orthogonal to the layers from image M00-02100, which was first straightened and then averaged along strike (Fig. 1). Concurrently acquired Mars Orbiter laser altimeter (MOLA) topographic data were used to convert the profiles of radiance as a function of pixel to radiance as a function of depth (Fig. 1). A clear feature in the first half of this profile is the presence of three nearly identical cycles (N1, N2 and N3 in Fig. 1), on top of which are some higher-frequency variations.

The age of the north polar layered terrain is currently poorly constrained. Viking observations suggested a net 0.02 to 0.08 cm annual water loss from the north cap[15], but recent analysis suggests the cap is near equilibrium[16]. The lower elevation of the north cap predicts a long-term average transport and accumulation of water at the north pole with respect to the south pole[7,16,17]. The present retention of CO_2 frost on the south cap alters this relationship, but this may not represent the average behaviour over the last million years[17]. On the basis of crude estimates of dust deposition rates, accumulation rates ranging from about 10^{-3} to 10^{-2} cm yr^{-1} have been proposed[5,6,18]. In contrast, the lack of any impact craters over 300 m in diameter led Herkenhoff and Plaut[7] to estimate the age of the surface at less than 120,000 yr, corresponding to a resurfacing rate of 0.1 to 0.2 cm yr^{-1}. As the total thickness of section we analyse

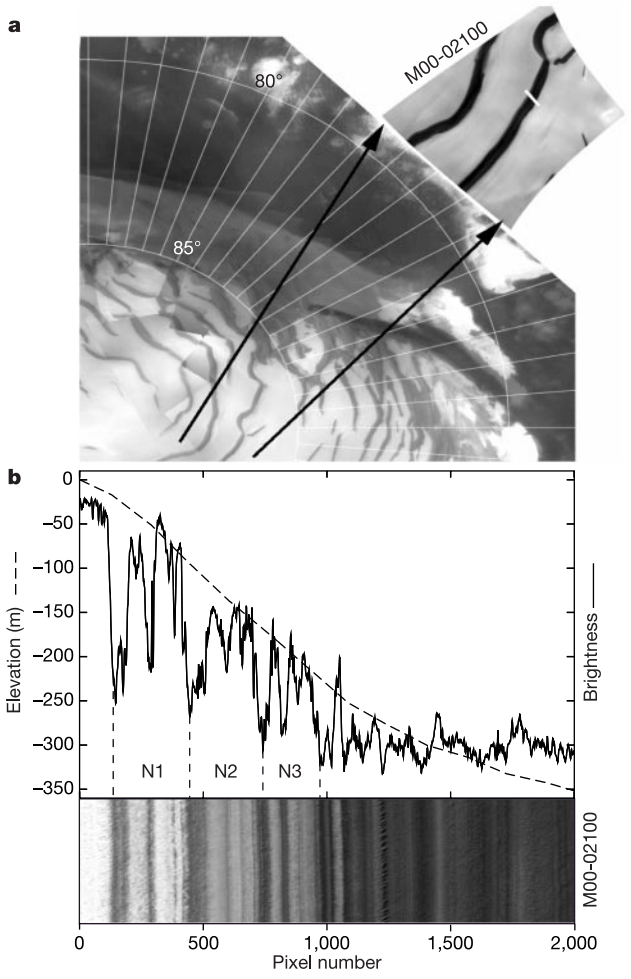

Figure 1 North pole layered terrains. **a**, Regional mosaic of Mars Orbiter camera (MOC) wide-angle camera images of the martian north pole showing the location of MOC narrow-angle image M00-02100. Circles of latitude 80° and 85° are plotted. **b**, The brightness profile (solid curve) versus pixel number for a section of the MOC narrow-angle image M00-02100 (bottom), is obtained by averaging the pixel value along vertical lines. This picture was taken by the MOC on 13 April 1999 (solar longitude $L_S \approx 123°$), at latitude 86.48°. The original image was processed in order to straighten it. The dashed line is the elevation resulting from the Mars Orbiter laser altimeter (MOLA) experiment measurements (in metres on the *y* axis, with origin at pixel 0). MOLA data were used to convert the profile from horizontal distance along the *x* axis to depth. There are 13 MOLA spots across the image, and the elevation is interpolated between the topographic measurements. We observe three similar cycles (N_1, N_2, N_3) between pixels 100 and 1,000.

is about 350 m, we can estimate from published deposition rates that the formation time for our section ranges from 100,000 to 35,000,000 yr.

Cutts and Lewis[4] proposed hypothetical stratigraphic sequences using climatic models of deposition, but comparison with measurements of layers was not possible with Viking Orbiter images resolution[4], about 30–50 times lower than the MOC (with up to 1.5 m pixel^{-1}). Here we directly compare the brightness profile of Fig. 2 to the north pole summer insolation in order to constrain the possible age of the deposit.

The changes in insolation at the surface of Mars arise from the variation of the planet's orbit resulting from the secular perturbations of all the other planets in the Solar System (see for example, ref. 19), and from the precession and obliquity variations of the spin axis of the planet. The orbital motion is obtained through a new numerical integration of the whole Solar System, including all nine main planets, the Moon as a separate object, Earth and solar oblateness, tidal dissipation in the Earth–Moon system and the effect of general relativity. This new solution was also adjusted and compared to the JPL ephemeris DE406 (ref. 20). For Mars, the maximum discrepancy in longitude over 3,000 yr (the range of DE406) is less than 0.2 arcsec, and 3×10^{-8} in eccentricity. The obliquity and precession of the Mars axis were computed using initial conditions deduced from the Pathfinder mission[21]. The most striking feature of the solution (Fig. 2) is that at about 5 Myr, the obliquity increases, reaching more than 45° which induces a large increase of the summer insolation in the north pole. The main uncertainty in the obliquity solution arises from the initial precession frequency ($p = -7.576 \pm 0.035$ arcsec yr^{-1} (ref. 21)). We have verified that even when doubling this uncertainty ($p = -7.576 \pm 0.070$ arcsec yr^{-1}) all solutions within this range lead to a similar increase of obliquity after 5 Myr, and behave as in Fig. 2d over 10 Myr, the chaotic behaviour of the solution[19,22,23] being only significant beyond 10 Myr.

To compare the photometric profile with insolation, the trend of radiance that appears to be strongly correlated with depth (Fig. 1) is removed and the data are scaled, resulting in the radiance profile shown in Fig. 3. We assume that the top of the section has an age of 0, although possible deviations of a few thousand years should not significantly affect our results.

The shortest possible timescale present in the insolation curve is related to the climatic precession with a period of about 51,000 yr, while the main period in obliquity is of about 120,000 yr, and 95,000 to 99,000 yr in eccentricity, with a strong modulation of period 2.4 Myr owing to the near resonance of the secular proper modes g_3

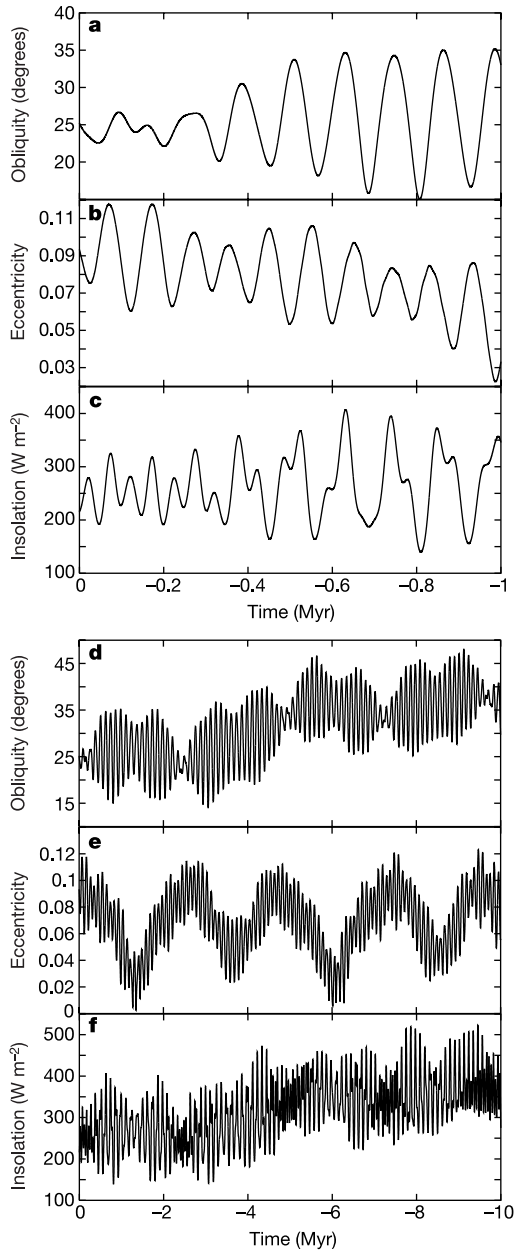

Figure 2 Obliquity, eccentricity and insolation at the north pole surface at the summer equinox ($L_S = 90°$). **a**–**c**, Over 1 Myr; **d**–**f**, over 10 Myr. The orbital data are the result of a numerical integration of the whole Solar System, including the Moon, Pluto, tidal dissipation terms, solar and Earth oblateness. In the first 0.5 Myr of **c**, as the obliquity variations are small, the insolation is dominated by precession, while in the remaining part, the insolation variations becomes dominated by the obliquity cycle. (These data are available by request to J.L.)

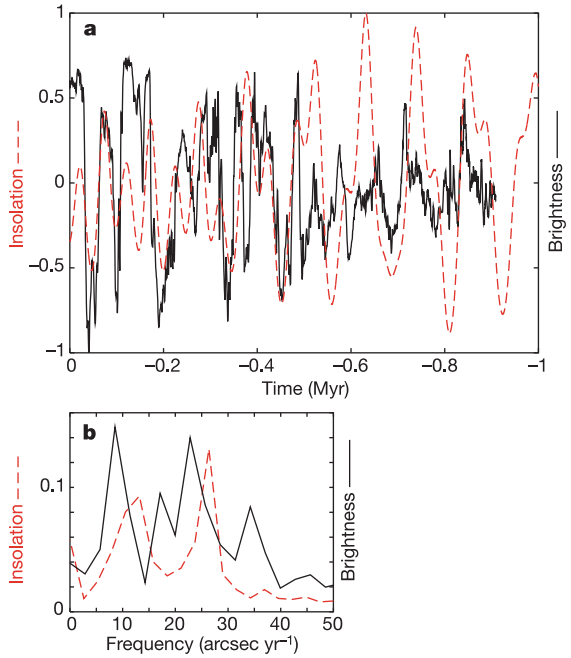

Figure 3 Comparison of brightness profile with insolation. **a**, Best fit of the brightness pattern from Fig. 1 (solid black curve) to the summer insolation at the north pole (Fig. 2c) (dotted red curve), after a transformation from pixel data to depth through the MOLA altimetry curve (Fig. 1) and, for the data beyond pixel 1,000, a division by 2 of the deposition rate. **b**, Spectral analysis of the insolation (dotted red) and the brightness pattern (solid black) over 0.5 Myr. Two main peaks are identified in both data. Owing to the short time span, in the insolation spectrum, the eccentricity and obliquity main frequencies are merged into a single line around 10 arcsec yr^{-1}. The second peak of the insolation curve (red) corresponds to climatic precession frequency (25.4 arcsec yr^{-1}).

and g_4 (refs 19, 24).

Owing to the weak constraint imposed by the deposition models, a large variety of timescales are possible, but we are able to rule some of them out. For example, if we try to associate the 2.4-Myr eccentricity period (Fig. 2e) to the main cycles of Fig. 1, the third cycle (from pixel 700 to 1,000) will span from 6 Myr to 8 Myr. But in this range, the obliquity, and thus the summer insolation, becomes very high (Fig. 2d, f). For obliquity of about 45°, the sublimation rate becomes so large ($\simeq$10 cm yr^{-1}) that the whole ice cap may be evaporated in about 10,000 yr (ref. 25), unless some dark residual deposit acts as a barrier for this evaporation[2]. In any case, it is thus doubtful that the response pattern of the ice deposit will be the same during the first low obliquity cycle and this high obliquity cycle. We therefore discarded this possibility, and preferred to consider that the shortest significant period in the pattern corresponds to the precession cycle, as it appears in the insolation curve in Fig. 2c. In this case, we recover a very good agreement between the first three photometric cycles and the three insolation cycles up to about 500,000 yr. In addition, the spectral analysis of the first 0.5 Myr of the insolation curve and the data (Fig. 3) reveal in both cases two main peaks at very close locations, supporting our analysis.

Although we considered only the average deposition rate for the transfer function from depth to time, short scale variations of this deposition rate should not significantly affect our results. Moreover, a significant change of deposition rate with insolation[2,17,25] would not change the main frequencies of the response, but only add additional harmonics, which could very well be present. Major erosional episodes may have caused unconformities and discontinuities in the layer accumulation[3], but on the basis of the regular layer expression and periodic patterns in the N_1, N_2 and N_3 cycles, we assumed that such large unconformities are not present in this first part of the record.

After 0.5 Myr, the amplitude of the obliquity (and thus also insolation) variations increase significantly. We assumed that the sublimation of the ice was larger during these periods, and thus that the effective deposition rate was smaller. In the same way, the decrease in atmospheric pressure at small obliquities will decrease the frequency and intensity of dust storms[2]. We expressed this hypothesis by dividing by an empirical factor of 2 the deposition rate in our transfer function from MOLA topography to time.

The photometric curve is then directly compared with the insolation curve in Fig. 3, with a very satisfactory agreement, compared to usual Earth palaeoclimate records[10–12]. With this process, we find that the time span for the whole 350 m layer is 900,000 yr. The first three main cycles, spanning 250 m, are accumulated in 500,000 yr, which corresponds to a deposition rate of 0.05 cm yr^{-1}, whereas in the remaining 400,000 yr, this value decreases to about 0.025 cm yr^{-1}.

The conjunction of high radiance level with high insolation value in summer fitted slightly better than the opposite (which would not change the timescale, but induces a shift of about 25,000 yr on the whole set). In fact, the deposition mechanism is not well known[26], and both hypotheses are possible. In the former, which we prefer, during the last precession-dominated 0.5 Myr (Fig. 3), the northern winter deposits are darkened by the most intense dust storm activity resulting from high summer insolation in the southern hemisphere (that is, low summer insolation in the northern hemisphere)[27,28]. In the second scenario, the dark bands are the result of ice sublimation due to high insolation in summer at the north pole. When the obliquity forcing becomes dominant (after 0.5 Myr), the scenario may change, but we preferred here to focus on the first part of the record, where the signal is most apparent.

It is clear that additional data would be welcome to firmly establish this timescale for the north polar deposit, although the proposed timescale best fits the available data with minimal adjustments; however, we are very far from being able to core the martian ice caps as was successfully done on the Earth[12]. As we had to slightly modify the deposition rate during the second part of the record, we consider the timescale for the first part, where the photometric signal is the strongest, to be more reliable than that obtained in the second part. Finally, we stress again that the depositional/erosional mechanisms for the formation of the polar caps remain highly unconstrained. We also leave as an open question whether the observed 3-km-thick north polar cap[29] could have been formed during the recent 5-Myr period of low obliquity, which would correspond to an average deposition rate close to our 0.05 cm yr^{-1} value. □

Received 8 April; accepted 8 August 2002; doi:10.1038/nature01066.

1. Murray, B. C. *et al.* Geological framework of the south polar region of Mars. *Icarus* **17,** 328–345 (1972).
2. Toon, O. B., Pollack, J. B., Ward, W., Burns, J. A. & Bilski, K. The astronomical theory of climatic changes of Mars. *Icarus* **44,** 552–607 (1980).
3. Howard, A. D., Cutts, J. A. & Blasius, K. R. Stratigraphic relationships within martian polar-cap deposits. *Icarus* **50,** 161–215 (1982).
4. Cutts, J. A. & Lewis, B. H. Models of climatic cycles record in Martian polar layered deposits. *Icarus* **50,** 216–244 (1982).
5. Pollack, J. B. *et al.* Properties and effects of dust particles suspended in the Martian atmosphere. *J. Geophys. Res.* **84,** 2929–2945 (1979).
6. Kieffer, H. H. H_2O grain size and the amount of dust in Mars residual north polar cap. *J. Geophys. Res.* **95,** 1481–1493 (1990).
7. Herkenhoff, K. & Plaut, J. J. Surface ages and resurfacing rates of the polar layered deposits on Mars. *Icarus* **144,** 243–253 (2000).
8. Malin, M. C. & Edgett, K. S. Mars Global Surveyor Mars Orbiter Camera: Interplanetary cruise through primary mission. *J. Geophys. Res.* **106,** 23429–23570 (2001).
9. Smith, D. E. *et al.* Mars Orbiter Laser Altimeter: Experiment summary after the first year of global mapping of Mars. *J. Geophys. Res.* **106,** 23689–23722 (2001).
10. Hays, J. D., Imbrie, J. & Schackleton, N. J. Variations of the Earth's orbit: Pacemaker of the ice ages. *Science* **194,** 1121–1132 (1976).
11. Imbrie, J. *et al.* On the structure and origin of major glaciation cycles: 1. Linear responses to Milankovitch forcing. *Paleoceanography* **7,** 701–738 (1992).
12. Petit, J. R. *et al.* Climate and atmospheric history of the past 420,000 years from the Vostok ice core, Antarctica. *Nature* **399,** 429–436 (1999).
13. Smith, D. E., Zuber, M. T. & Neumann, G. A. Seasonal variations of snow depth of Mars. *Science* **294,** 2141–2145 (2001).
14. Blasius, K. R., Cutts, J. A. & Howard, A. D. Topography and statigraphy of martian polar layered deposits. *Icarus* **50,** 140–160 (1982).
15. Haberle, R. M. & Jakosky, B. M. Sublimation and transport of water from the north polar residual cap on Mars. *J. Geophys. Res.* **95,** 1423–1437 (1990).
16. Richardson, M. I. & Wilson, R. J. A topographically forced assymetry in the martian circulation and climate. *Nature* **416,** 298–301 (2002).
17. Jakosky, B. M., Henderson, B. G. & Mellon, M. T. The Mars water cycle at other epochs: Recent history of the polar caps and layered terrain. *Icarus* **102,** 286–297 (1993).
18. Cantor, B. A., James, P. B., Caplinger, M. & Wolff, M. J. Martian dust storms: 1999 Mars Orbiter Camera observations. *J. Geophys. Res.* **106,** 23653–23687 (2001).
19. Laskar, J. The chaotic motion of the solar system. A numerical estimate of the size of the chaotic zones. *Icarus* **88,** 266–291 (1990).
20. Standish, E. M. JPL Planetary and Lunar Ephemerides, DE405/LE405. (Jet Propulsion Laboratory Inter Office Memorandum, 312.F-98-048, 1998).
21. Folkner, W. M., Yoder, D. N., Yuan, E. M., Standish, E. M. & Preston, R. A. Interior structure and seasonal mass redistribution of Mars from radio tracking of Mars Pathfinder. *Science* **278,** 1749–1752 (1997).
22. Laskar, J. & Robutel, P. The chaotic obliquity of the planets. *Nature* **361,** 608–612 (1993).
23. Touma, J. & Wisdom, J. The chaotic obliquity of Mars. *Science* **259,** 1294–1297 (1993).
24. Laskar, J. The limits of Earth orbital calculations for geological time scale use. *Phil. Trans. R. Soc. Lond. A* **357,** 1735–1759 (1999).
25. Jakosky, B. M., Henderson, B. G. & Mellon, M. T. Chaotic obliquity and the nature of the Martian climate. *J. Geophys. Res.* **100,** 1579–1584 (1995).
26. Thomas, P., Herkenhoff, K., Howard, A., Murray, B. & Squyres, S. in *Mars* (eds Kieffer, H. H., Jakosky, B. M., Snyder, C. W. & Matthews, M. S.) 767–795 (Univ. Arizona Press, Tucson, 1992).
27. Paige, D. A. & Ingersoll, P. Annual heat balance of Martian polar caps: Viking observations. *Science* **228,** 1160–1168 (1985).
28. Martin, L. J. & Zurek, R. W. An analysis of the history of dust storm activity on Mars. *J. Geophys. Res.* **98,** 3221–3246 (1993).
29. Zuber, M. T. *et al.* Observations of the north polar region of Mars from the Mars Orbiter Laser altimeter. *Science* **282,** 2053–2060 (1998).

Acknowledgements

We thank F. Forget, A. Howard and B. Jakosky for useful discussions and suggestions, and A. Correia and M. Gastineau for their contribution to the obliquity solution. This work was supported by the CNRS-PNP and NASA Solar System Exploration programmes.

Competing interests statement

The authors declare that they have no competing financial interests.

Correspondence and requests for materials should be addressed to J.L. (e-mail: laskar@bdl.fr).